Geoscience Letters

RESEARCH LETTER

Open Access

Two-year consecutive concurrences of positive Indian Ocean Dipole and Central Pacific El Niño preconditioned the 2019/2020 Australian "black summer" bushfires

Guojian Wang[1,2] and Wenju Cai[1,2*]

Abstract

The 2019/20 Australian black summer bushfires were particularly severe in many respects, including its early commencement, large spatial coverage, and large number of burning days, preceded by record dry and hot anomalies. Determining whether greenhouse warming has played a role is an important issue. Here, we examine known modes of tropical climate variability that contribute to droughts in Australia to provide a gauge. We find that a two-year consecutive concurrence of the 2018 and 2019 positive Indian Ocean Dipole and the 2018 and 2019 Central Pacific El Niño, with the former affecting Southeast Australia, and the latter influencing eastern and northeastern Australia, may explain many characteristics of the fires. Such consecutive events occurred only once in the observations since 1911. Using two generations of state-of-the-art climate models under historical and a business-as-usual emission scenario, we show that the frequency of such consecutive concurrences increases slightly, but rainfall anomalies during such events are stronger in the future climate, and there are drying trends across Australia. The impact of the stronger rainfall anomalies during such events under drying trends is likely to be exacerbated by greenhouse warming-induced rise in temperatures, making such events in the future even more extreme.

Keywords: 2019/20 Australian bushfires, Positive Indian Ocean Dipole, Central Pacific El Niño, Climate change

Introduction

Eastern and southeastern Australia experience bushfires almost every year (Cai et al. 2009a), but the 2019/2020 season are particularly severe. Referred to as the "Black Summer," the 2019 fires commenced in June 2019 in northeastern Australia, and saw a large area of forest burnt out of control between September 2019 and March 2020 in New South Wales, Victoria, Australia Capital Territory, and other southeastern Australia regions. By early March, the estimated loss included a burnt area of 180,000 square kilometres, at least 34 people killed, one billion animals perished, and 59,000 buildings destroyed. The economic cost amounted to billions, exceeding that of the Black Saturday bushfires, 7 February 2009 in Southeastern Australia, not counting the health impact arising from the associated hazardous air quality within Australia and in regions downstream as remote as South America, affecting millions of people. In addition, more than 300 million tonnes of CO_2 were emitted, more than 50% of Australia's annual emissions, contributing to a long-term climatic impact. Whether greenhouse warming played a role is an issue commonly raised.

Eastern and southeastern Australia climate is influenced by modes of tropical climate variability, which include the Indian Ocean Dipole (IOD) (Saji et al. 1999; Ashok et al. 2003; Cai et al. 2009a; Ummemhofer et al.

*Correspondence: Wenju.Cai@csiro.au
[1] Key Laboratory of Physical Oceanography–Institute for Advanced Ocean Studies, Ocean University of China and Qingdao National Laboratory for Marine Science and Technology, Yushan Road, Qingdao 266003, China
Full list of author information is available at the end of the article

2009; Min et al. 2013) and El Niño events (Nicholls et al. 1996), particularly central Pacific (CP) El Niño (Ashok et al. 2007; Wang and Hendon 2007; Taschetto and England 2009). A positive IOD (pIOD), with cold sea surface temperature (SST) anomalies in the equatorial eastern Indian Ocean usually starts to develop in austral winter June-July-August (JJA). The associated anomalously low convective heating in the eastern Indian Ocean generates eastern Indian Ocean Rossby wave trains with a high sea level pressure centre south of Australia, inducing an anomalous dry condition over southern and southeastern Australia (Cai et al. 2011) (Fig. 1a). As the pIOD matures into austral spring (September-October-November, SON) the Rossby wave trains intensify and shift westward, and the low rainfall anomalies persist over much of the southern Australia, including a decrease in southwest Western Australia (Fig. 1b). In JJA, the impact of a central Pacific El Niño occurs over much of eastern and northeastern Australia (Fig. 1c) when the western Pacific convection shifts eastward. In SON the impact intensifies and is felt in a broader northern Australia and southeast Australia (Fig. 1d) owing to CP-El Niño's coherence with the pIOD, because El Niño does not have a direct dynamical pathway to influence southern Australia (Cai et al. 2011). During either pIOD or CP-El Niño, as rainfall decreases, cloud cover reduces, thus surface temperature increases in the affected regions (Cai et al. 2009a), increasing evaporation, which accelerates depletion of soil moistures (Cai et al. 2009b).

In this paper, we show that the anomalous climate condition underpinning the 2019/20 Australia fires is a set of consecutive concurrent pIOD and CP-El Niño events that favour a large spatial scale of dry conditions for bushfires and their early commencement. We then assess the frequency of such consecutive occurrences and their response to greenhouse condition using climate models.

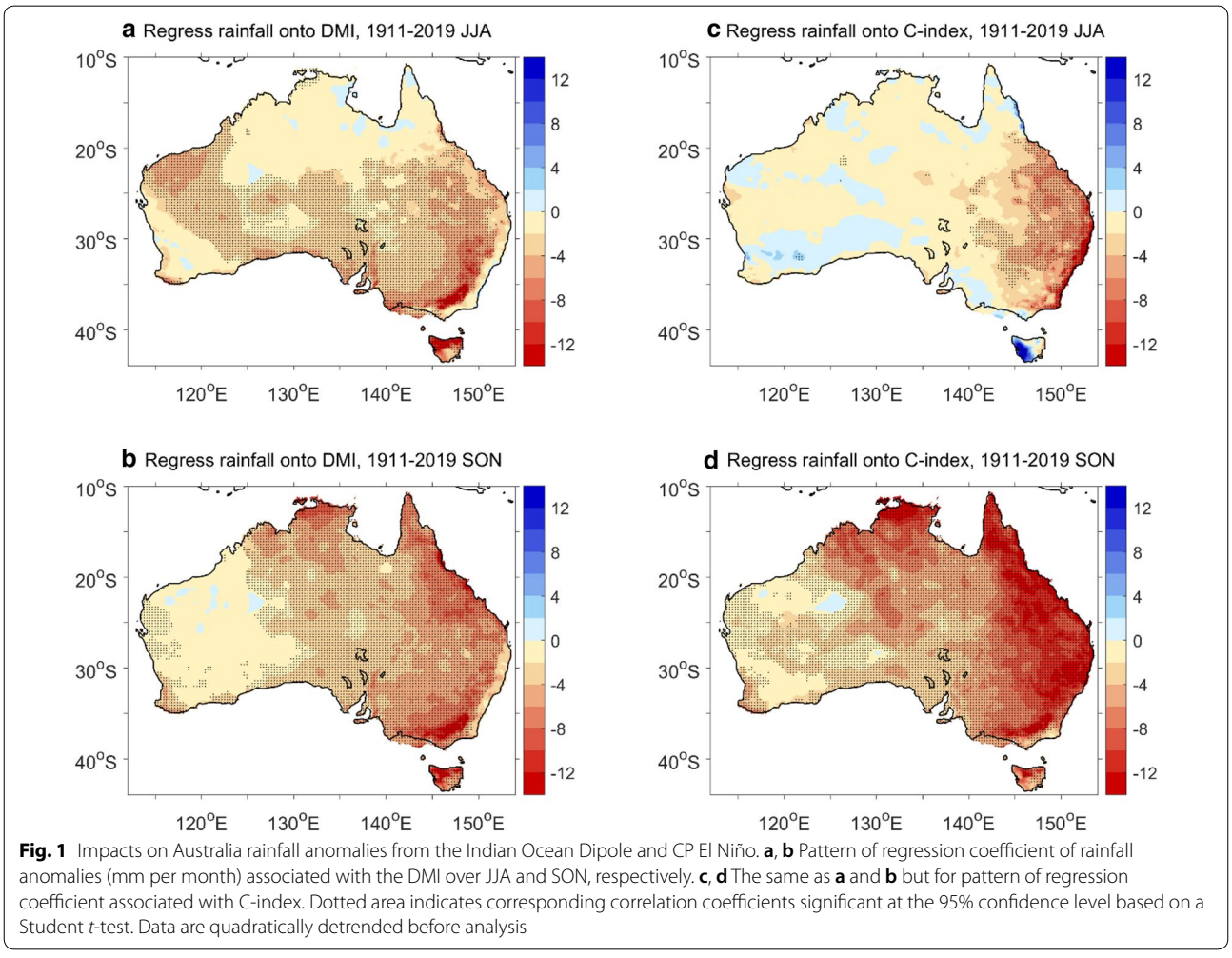

Fig. 1 Impacts on Australia rainfall anomalies from the Indian Ocean Dipole and CP El Niño. **a**, **b** Pattern of regression coefficient of rainfall anomalies (mm per month) associated with the DMI over JJA and SON, respectively. **c**, **d** The same as **a** and **b** but for pattern of regression coefficient associated with C-index. Dotted area indicates corresponding correlation coefficients significant at the 95% confidence level based on a Student *t*-test. Data are quadratically detrended before analysis

Data and indices of the IOD and CP-El Niño

We use rainfall data from the Australia Landscape Water Balance (Australian Water Resource Assessment Landscape, or AWRA-L) Model, which is a 0.05° (approximately 5 km) gridded daily water balance model developed by CSIRO and the Australian Bureau of Meteorology for Water Resource assessment purposes (see Hafeez et al. 2015; Viney et al. 2015; and Van Dijk et al.2010 for the model description). The outputs are already widely used by state and commonwealth water and agriculture agencies for water resource assessment and planning, agriculture and natural resource management, flood applications and groundwater modelling applications across Australia.

To elucidate influences from the IOD, we use the dipole mode index (DMI; Saji et al. 1999) which describes difference in SST between the tropical western (50°E-70°E, 10°S-10°N) and eastern Indian Ocean (90°E-110°E, 10°S-0°); for impacts from CP-ENSO, we use index constructed from an empirical orthogonal function (EOF) analysis on quadratically detrended monthly SST anomalies (Takahashi et al. 2011) over the tropical Pacific region (140°E-80°W, 15°S-15°N). This is based on monthly SST data from Hadley Centre Sea Ice and Sea Surface Temperature dataset version 1.1. (HadISST v1.1) (Rayner et al. 2003) from 1911 onward, to match the Australia rainfall data length. The EOF analysis gives two dominant modes, the first one with a spatial pattern featuring warming in the eastern, and the second mode with warming in the central Pacific, each with a principal component (PC) time series scaled to unity. The C-index is described as $(PC1+PC2)/\sqrt{2}$, which represents SST variability over the anomaly centre in the central Pacific Ocean. The greater the C-index, the warmer the SST anomalies in the CP region. The other ENSO regime, i.e., EP ENSO regime, is described by an E-index, $(PC1-PC2)/\sqrt{2}$, which represents SST variability over the anomaly centre in the eastern Pacific Ocean. In this study, we focus on impacts from CP-ENSO regime.

To evaluate projected changes in frequency of 2-year consecutive concurrence of pIOD and CP-El Niño, and the associated rainfall anomalies over Australia, we examine a total of 17 CMIP5 coupled general circulation models forced with historical anthropogenic and natural forcings before 2005 and future greenhouse warming under the RCP8.5 emission scenario (Taylor et al. 2012) thereafter to 2099. The 17 models are selected based on their ability to simulate a reasonable ENSO diversity, i.e., distinguishable CP-ENSO and EP-ENSO regimes (Cai et al. 2018; Wang et al. 2020). Rainfall, surface temperature and SST are utilised. We also used data from 23 CMIP6 models based on the same selection criterion. The CMIP6 models are forced by historical forcing up to 2014 and thereafter the shared socioeconomic pathway 5–8.5 emission scenario, which is approximately equivalent to RCP8.5 (Eyring et al. 2016). See Table 1 for more information of the selected models from CMIP5 and CMIP6.

Rare consecutive occurrence of pIOD and CP-El Niño events

During the five austral winters since 2015, the JJA C-index show five consecutive years of seasonal positive surpassing a 0.5 standard deviation (s.d.) value with three winters superimposed by a positive IOD index exceeding 0.5 s.d. (Fig. 2a). Such consecutive events have a cumulative depleting impact on soil moisture (Cai et al. 2009a, b). Throughout the 110 years of evolution, there was only another such five consecutive years of C-index, which took place during 1991–1995 with two superimposing pIOD events including the extreme 1994 event. Further, time series of SON IOD index and CP-ENSO index shows that although

Table 1. 17 CMIP5 models and 23 CMIP6 models that produce reasonable nonlinearity (half of the observed) between PC1 and PC2

CMIP5	α	CMIP6	α
FIO-ESM	− 0.5155	CAMS-CSM1-0	− 0.2902
GISS-E2-R	− 0.1995	FGOALS-f3-L	− 0.5547
bcc-csm1-1-m	− 0.2518	FGOALS-g3	− 0.3096
CCSM4	− 0.3245	CMCC-CM2-SR5	− 0.4055
CESM1-BGC	− 0.1776	CNRM-CM6-1	− 0.1662
CESM1-CAM5	− 0.3953	CNRM-ESM2-1	− 0.1687
CMCC-CESM	− 0.2502	EC-Earth3	− 0.2662
CMCC-CM	− 0.1872	EC-Earth3-Veg	− 0.2665
CMCC-CMS	− 0.3155	FIO-ESM-2–0	− 0.3751
CNRM-CM5	− 0.1738	MIROC6	− 0.3198
FGOALS-s2	− 0.2142	MIROC-ES2L	− 0.3466
GFDL-CM3	− 0.2931	HadGEM3-GC31-LL	− 0.1785
GFDL-ESM2M	− 0.3882	MPI-ESM1-2-h	− 0.2660
GISS-E2-H	− 0.1789	MPI-ESM1-2-LR	− 0.2338
IPSL-CM5B-LR	− 0.2594	MRI-ESM2-0	− 0.3387
MIROC5	− 0.3605	GISS-E2-1-G	− 0.3644
MRI-CGCM3	− 0.1583	CESM2	− 0.3216
		CESM2-WACCM	− 0.2436
		NorESM2-LM	− 0.2505
		NorESM2-MM	− 0.2077
		GFDL-ESM4	− 0.1931
		CIESM	− 0.1886
		MCM-UA-1-0	− 0.2888

Here we use $\boldsymbol{\alpha}$ to indicate the strength of the nonlinear relationship as in $PC2(t) = \boldsymbol{\alpha}\, PC1(t)^2$. (see Data session; see also Cai et al. 2018). The observed $\boldsymbol{\alpha}$ based on multi-products as in Cai et al. (2018) is -0.31. The more negative in $\boldsymbol{\alpha}$, the higher nonlinearity in the ENSO system

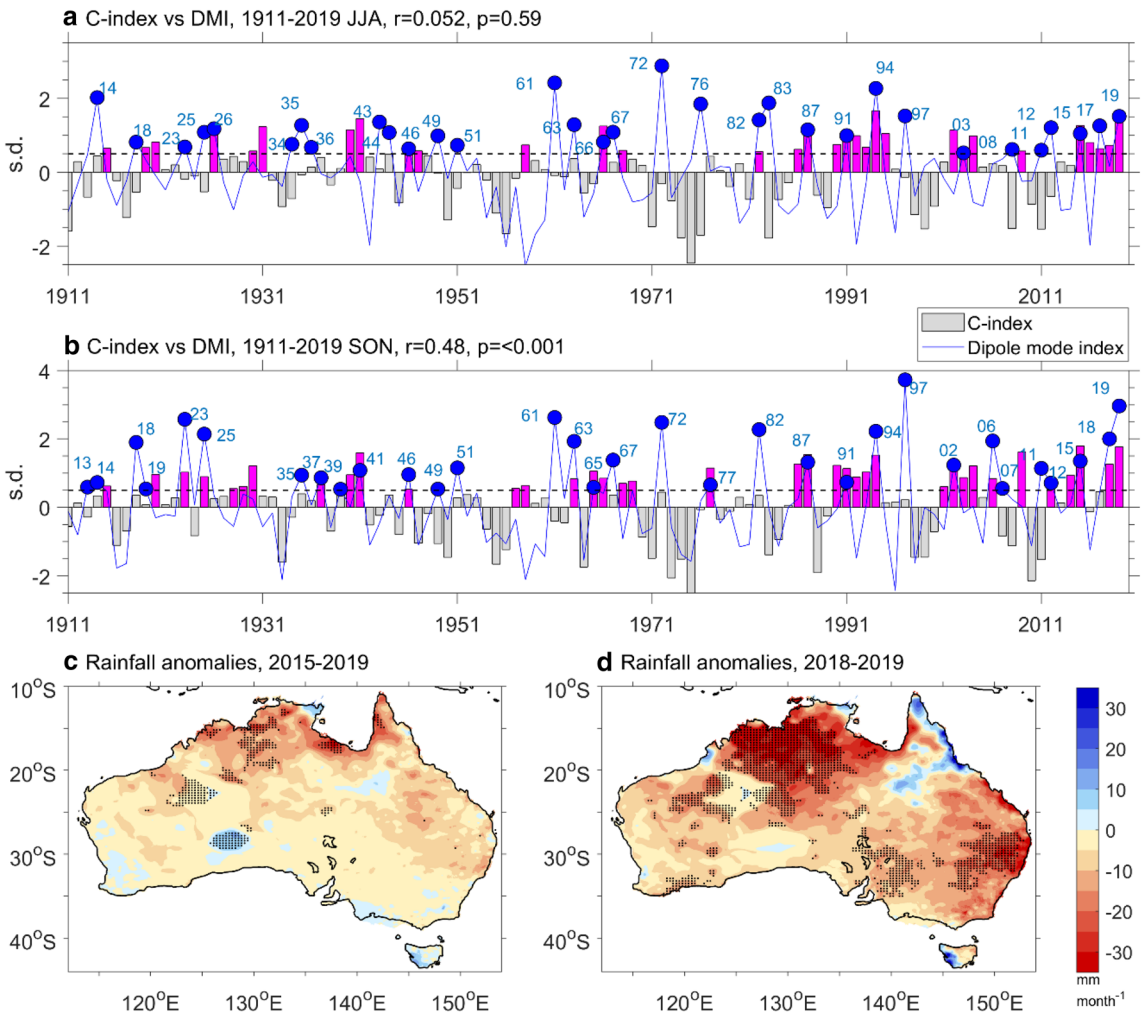

Fig. 2 The consecutive concurrences of CP El Niño and pIOD event and the recent severe drought over Australia. **a** A comparison between the JJA C-index (bars) and the JJA DMI (blue curve) from 1911 to 2019. The pink bars highlight CP El Niño years defined as when the C-index is greater than 0.5 s.d.; and a positive IOD event indicated by blue filled circle is defined as when the DMI is greater than 0.5 s.d. The correlation coefficient and *p* value are shown on the title. **b** The same as **a** but for the SON season. **c** Mean monthly rainfall anomalies over the recent five years, i.e., from 2015 to 2019. **d**, The same as **c** over the recent two years, i.e., from 2018 to 2019. Data are quadratically detrended before analysis. Dotted areas indicate regions where the anomalies are greater than a 2.0 s.d. value of the 5 year and 2 year running time series at each grid-points in **c** and **d**, respectively

single-year concurrent pIOD and CP-El Niño events occur relatively often (for example, in terms of SON indices: 1923, 1925, 1937, 1941, 1946, 1963, 1965, 1977, 1987, 1991, 1994, 2002, 2006, 2012, 2015, 2018, 2019), on average about one in 5 years, there is only one such 2-year consecutive concurrence, that is, during 2018/2019, throughout the entire time series (Fig. 2b). This suggests an overall dry period across eastern and southeastern Australia over the past five years and particularly last two years (Fig. 2c, d). Note that, the following results do not change if different SON C-index threshold values, e.g., greater than 1.0 s.d., are used to define consecutive events.

The rarity of the sequence in the JJA and SON time series provides a relevant context for understanding the unique characteristics of the 2019/20 fire season, which transcends the large spatial scale. The consecutive CP El Niño events provide a conducive environment for the 2019 fire seasons to commence in northeastern Australia in JJA, a dry season, made worse by the negative

rainfall anomalies due to the 2018 CP-El Niño and the soil moisture-depleting period, or early in SON in eastern Australia. Over southeastern Australia, cumulative effect from the consecutive 2018 and 2019 pIOD events likewise provides a favourable condition for bushfires to occur in early austral summer, a dry season when bushfires normally take place. Rainfall and temperature station data from the Australian Bureau of Meteorology show that in many parts of the eastern and southeastern Australia, not only record dry in terms of two-year cumulative rainfall anomalies (for example, greater than 2.s.d., stippled area in Fig. 2d), but record warm conditions were observed, which exacerbated the effect of the extreme dry condition. Together, these anomalies create a "perfect" condition for the devastating fires, spatially expansive from north to south of the country, long-lasting from winter to summer, and with an extreme ferocity that is rarely seen.

Apart from the high temperatures, which are contributed by long-term warming trends, does greenhouse warming contribute to the generation of the 2-year consecutive concurrent pIOD and CP-El Niño events? Below we examine climate models participating in the Coupled Model Inter-comparison Project Phase 5 (CMIP5) and Phase 6 (CMIP6) to address the issue.

Impact from greenhouse warming

We examine models participating in CMIP5 forced by historical and RCP8.5 emission scenario to 2099 (Taylor et al. 2012). The C-index for each model are obtained from EOF analysis on quadratically detrended monthly SST anomalies over the 200 years (1900–2099). We use 17 out of 34 CMIP5 that are better able to simulate nonlinear dynamical process and hence CP-ENSO as in Cai et al. (2018). Previous studies have found that there is no inter-model consensus on change in the IOD SST variability (Cai et al. 2013; Zheng et al. 2013; Hui and Zheng 2018), but an increase in CP-ENSO variability with a reasonable inter-model agreement (Cai et al. 2018). We compare the frequency of concurrences of a pIOD with CP-El Niño by comparing two 100-year periods that is, 1900–1999 (Control) and 2000–2099 (Future) focusing on events identified with SON indices.

As in the observed (Fig. 2b), there is a moderate correlation between the IOD and CP-ENSO as seen from Fig. 3a, b in both the Control and Future climate, consistent with previous examination (Cai et al. 2010). The total number of consecutive concurrent pair of pIODs and CP-El Niños is 52 over the 1700 years of virtual climate, that is, one pair in 33 years, more frequent than the observed in the model aggregation. The frequency increases to 64 per 1700 years, or one pair in 27 years. However, there is no inter-model consensus, with only 9 out of 17 models producing an increase. This result suggests that greenhouse warming may not have influenced the dynamical trigger of the consecutive concurrences of pIOD and CP-El Niño events in 2019/20. We also examined 23 CMIP6 models based on the same model selection criterion as for CMIP5 (see Table 1). Results are similar (Fig. 3c, d) to those of CMIP5 but suggest a higher climate sensitivity in CMIP6 (Zelinka et al. 2020).

Are the impacts on rainfall changing? To this end, we compare composites of raw rainfall anomalies. For each pair of concurrent events, we construct average of the JJA and SON rainfall anomalies over the four seasons of the two consecutive years. Multi-model averages of all pairs in terms of raw rainfall for the Control and Future climate show that there is greater drying in the Future climate across Australia (Fig. 4a, b). Composites of quadratically detrended rainfall anomalies generate a similar result but less intense (figure not shown). Thus, difference between Fig. 4a, b, or between Fig. 5a, b, largest in the western half of Australia, and smaller in the eastern half, is contributed by both greenhouse warming-induced drying trends (Figs. 4c, 5c), and by stronger anomalies during such events, particularly in CMIP6 (Fig. 5b). The forcing factors for the drying trends include a positive Southern Annular Mode (Shi et al. 2008; Wang and Cai 2013; Cai et al. 2010) that affects Southwestern West Australia and southern Australia, a faster warming in the tropical western Indian Ocean than the east, or a pIOD-like change that generates a reduction in the JJA and SON mean rainfall through a similar process whereby a pIOD exerts its influence on the southern and southeastern Australia (Shi et al. 2008), and an El Niño-like warming pattern in the equatorial Pacific affecting eastern Australia (Shi et al. 2008). Furthermore, the impact of the intensified drying will be exacerbated by the background warming of 2–4 °C across much of the Australian continent (Figs. 4d, 5d), which increases potential evaporation, and depletes soil moisture. Thus, greenhouse warming-induced drying trends and the intensified future rainfall anomalies is likely to make future two-year consecutive pIOD and CP-El Nino events more extreme in terms of rainfall deficit, and the projected rise in temperatures (Figs. 4d and 5d) will exacerbate the impacts.

Conclusions

During the 2019/20, Australia experienced a catastrophic bushfire unlike any previous years, with the expansive spatial scale from Brisbane to Tasmania, lasting over 6 months with an early commencement amid severe dry

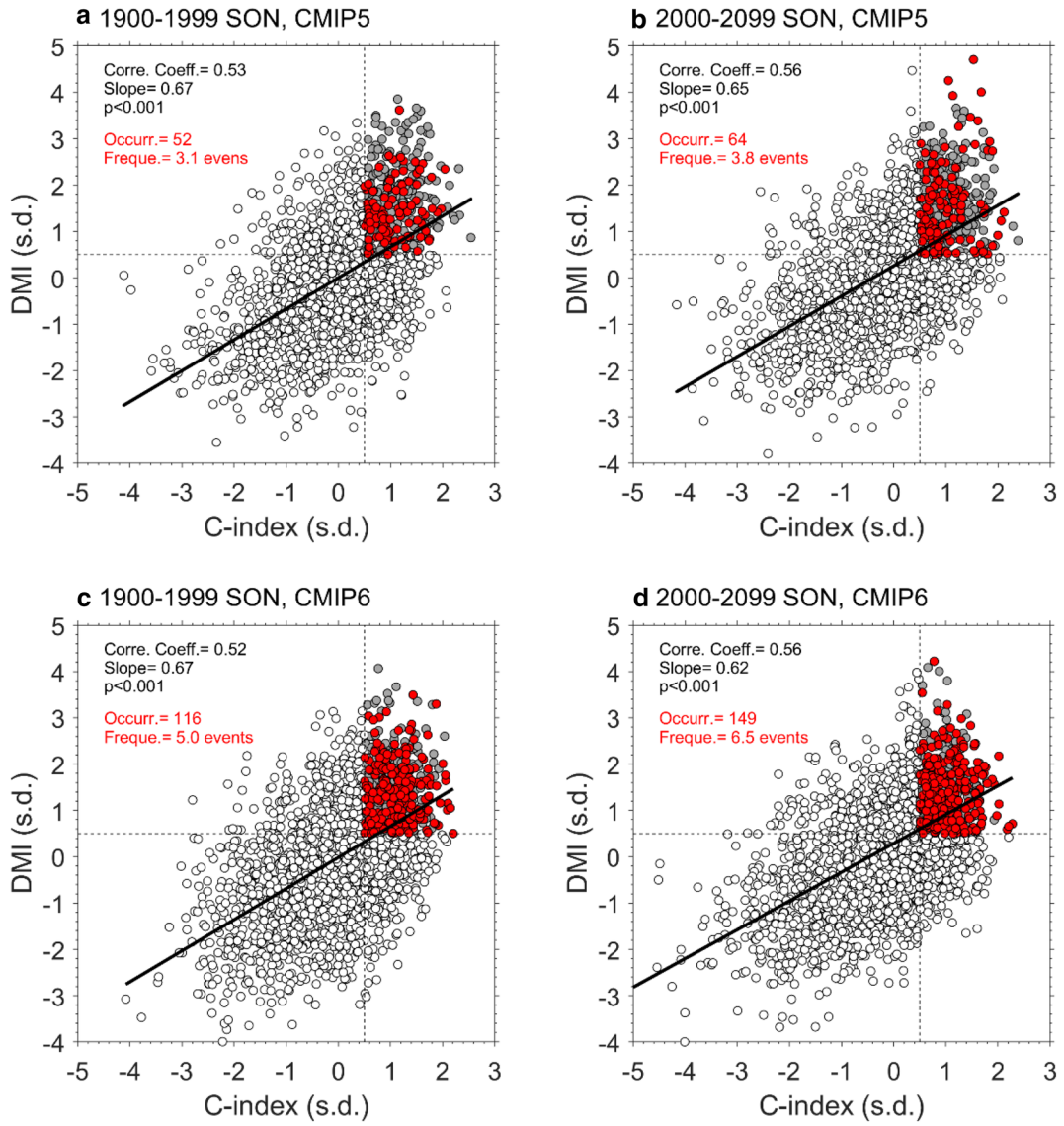

Fig. 3 Relationship between SON C-index and SON DMI. Show are based on outputs from 17 CMIP5 models for **a** the 1900–1999 and **b** the 2000–2099 periods and 23 CMIP6 models for **c** the 1900–1999 and d the 2000–2099 periods. See Table 1 for models that are selected for the analysis. Correlation, slope and p value are indicated in each panel. Red dots indicate events that are similar to 2018–2019 when consecutive concurrent pIOD (DMI is greater than 0.5 s.d.) and CP El Niño (C-index is greater than 0.5 s.d.) events occur for two years; dark grey dots indicate other concurrent pIOD and CP El Niño years. The total number of consecutive concurrences is indicated in red text. The associated frequency is also shown in each panel

and hot anomalies. We find that the two-year consecutive 2018 and 2019 pIOD events in conjunction with the consecutive 2018 and 2019 CP-El Niños, together with the warm condition conspired to provide a background condition that contributed to the extreme properties in terms of commencement time, long duration, and intensity. However, there is no strong modelling evidence to suggest that greenhouse warming contributed to the

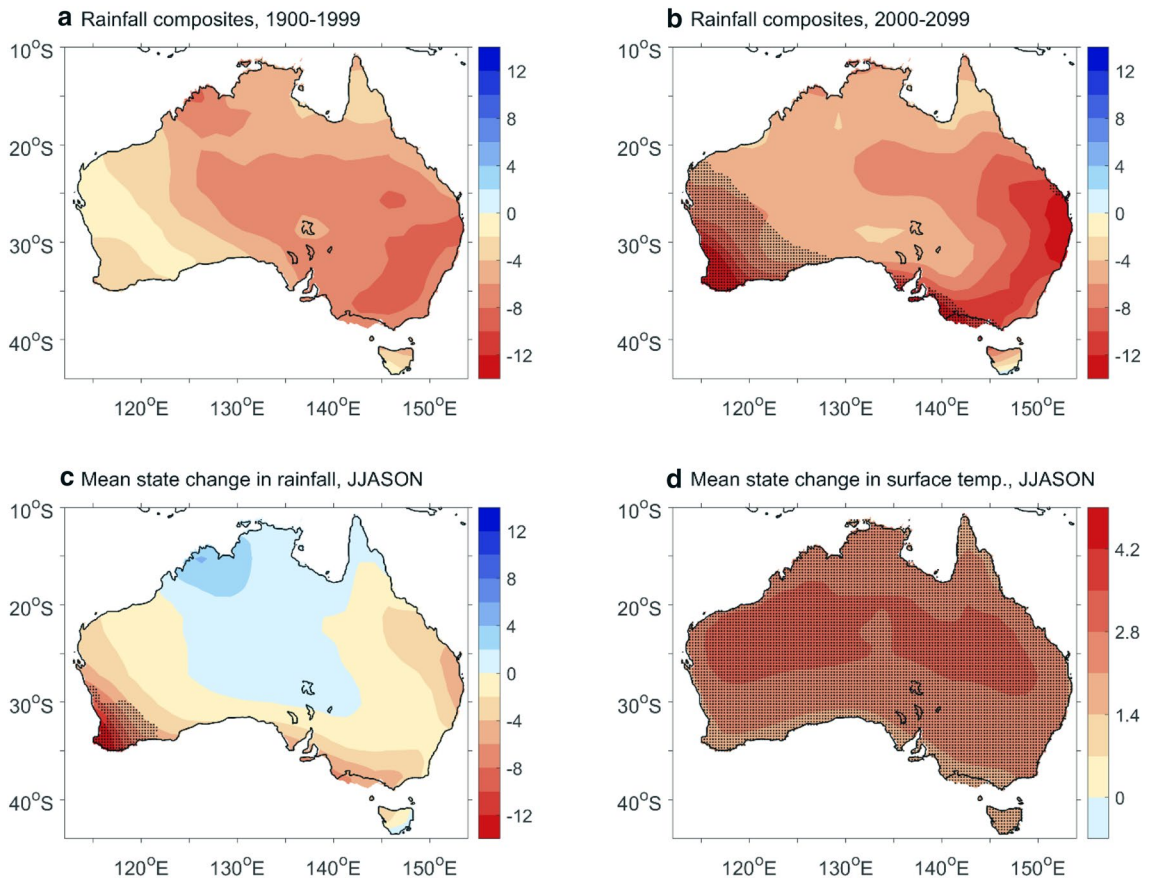

Fig. 4 Possible influences from mean state change under greenhouse warming based on CMIP5. **a** Composites of JJASON mean rainfall anomalies (mm per month) for events that are similar to 2018–2019 sequences in the Control climate, i.e., 1900–1999. **b** The same as **a**, but for the Future climate, i.e., 2000–2099. Dotted areas indicate where the difference between **a** and **b** is significant at the 95% confidence level based on a Student *t*-test. **c** Projected changes in Australia JJASON rainfall between 2000–2099 and 1900–1999. **d** The same as **c**, but in surface temperature (°C). Results are based on 17 CMIP5 models that produce reasonable ENSO diversity (Cai et al. 2018). Dotted area in **c** and **d** indicate where the difference between two period is significant above the 95% confidence level based on a Student t-test

triggering of the two-year consecutive pIOD and CP-El Niño occurrence, with both CMIMP5 and CMIP6 showing only a small increase in future occurrences. However, detrended rainfall anomalies tend to be stronger in the future, and there is a drying trend in the mean condition. Thus, the impact of future 2-year consecutive concurrences of CP-El Niños with pIODs similar to what we experienced in 2019/20 is likely to be more severe as the associated larger rainfall anomalies and dry trends are exacerbated by the rise in temperatures.

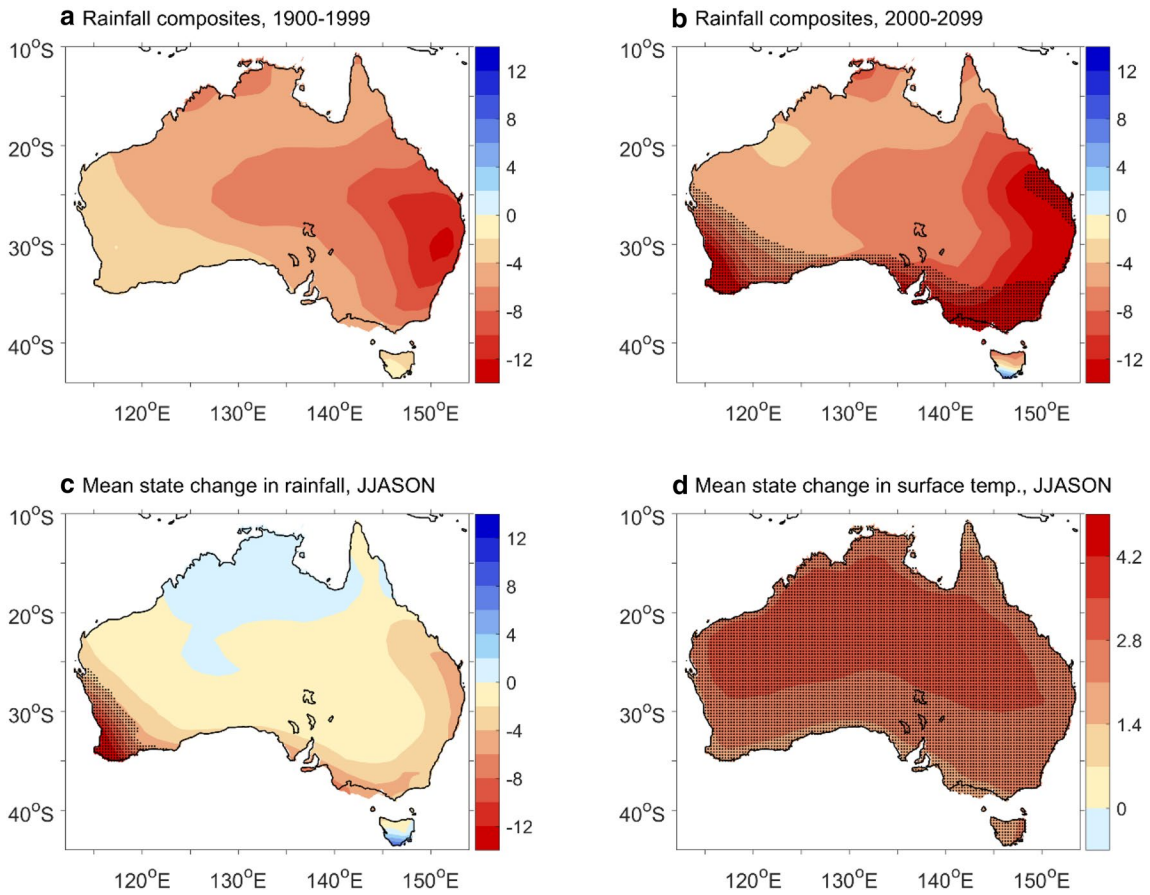

Fig. 5 Possible influences from mean state change under greenhouse warming based on CMIP6. **a** Composites of JJASON mean rainfall anomalies (mm per month) for events that are similar to 2018–2019 sequences in the Control climate, i.e., 1900–1999. **b** The same as **a**, but for the Future climate, i.e., 2000–2099. Dotted areas indicate where the difference between **a** and **b** is significant at the 95% confidence level based on a Student *t*-test. **c** Projected changes in Australia JJASON rainfall between 2000–2099 and 1900–1999. **d** The same as **c**, but in surface temperature (°C). Results are based on 23 CMIP6 models that produce reasonable ENSO diversity (Cai et al. 2018). Dotted area in **c** and **d** indicate where the difference between two period is significant above the 95% confidence level based on a Student *t*-test

Abbreviations

IOD: Indian Ocean Dipole; pIOD: Positive Indian Ocean Dipole; CP: Central Pacific; CMIP5: Coupled Model Inter-comparison Project Phase 5; CMIP6: Coupled Model Inter-comparison Project Phase 6; JJA: June, July and August; SON: September, October, and November; PC: Principal component; EOF: Empirical orthogonal function; DMI: Dipole mode index; s.d.: Standard deviation.

Acknowledgements

We thank Dr. Habibur Rahman who supplied Australia rainfall data. This work is supported by the Centre for Southern Hemisphere Oceans Research, a joint research centre between QNLM and CSIRO. W.C. and G. W. are also supported by the Earth Systems and Climate Change Hub of the Australian Government's National Environmental Science Program.

Authors' contributions

WC and GW conceived the study and wrote the manuscript. GW performed the analysis and generated the final figures. Both authors read and approved the final manuscript.

Funding

This work is supported by the Centre for Southern Hemisphere Oceans Research, a joint research centre between QNLM and CSIRO. W.C. and G.W. are also supported by the Earth Systems and Climate Change Hub of the Australian Government's National Environmental Science Program, and a CSIRO Office of Chief Executive Science Leader award.

Availability of data and materials

Australia rainfall data from Australia Landscape Water Balance are available on reasonable request to Dr. Habibur Rahman (habibur.rahman@bom.gov.au); HadISST are publicly available by accessing https://climatedataguide.ucar.edu/climate-data/sst-data-hadisst-v11; CMIP5 datasets are publicly available by accessing https://esgf-node.llnl.gov/projects/cmip5/; CMIP6 datasets are publicly available by accessing https://esgf-node.llnl.gov/projects/cmip6/.

Competing interests

The authors declare that they have no competing interests.

Author details

[1] Key Laboratory of Physical Oceanography–Institute for Advanced Ocean Studies, Ocean University of China and Qingdao National Laboratory for Marine Science and Technology, Yushan Road, Qingdao 266003, China. [2] Center for Southern Hemisphere Oceans Research (CSHOR), CSIRO Oceans and Atmosphere, Hobart 7004, Australia.

Received: 28 April 2020 Accepted: 20 October 2020
Published online: 10 November 2020

References

Ashok K, Guan Z, Yamagata T (2003) Influence of the Indian Ocean dipole on the Australian winter rainfall. Geophys Res Lett 30(15):1821. https://doi.org/10.1029/2003GL017926

Ashok K, Behera SK, Rao SA, Weng H, Yamagata T (2007) El Niño Modoki and its possible teleconnection. J Geophys Res 112:C11007. https://doi.org/10.1029/2006JC003798

Cai W, Cowan T, Raupach M (2009) Positive Indian Ocean dipole events precondition southeast Australia bushfires. Geophys Res Lett 36:L19710. https://doi.org/10.1029/2009GL039902

Cai W, Cowan T, Briggs P, Raupach M (2009) Rising temperature depletes soil moisture and exacerbates severe drought conditions across southeast Australia. Geophys Res Lett 36:L21709. https://doi.org/10.1029/2009GL040334

Cai W, Sullivan A, Cowan T (2010) Interactions of ENSO, the IOD, and the SAM in CMIP3 models. J Clim 24:1688–1704. https://doi.org/10.1175/2010JCLI3744.1

Cai W, van Rensch P, Cowan T, Hendon HH (2011) Teleconnection pathways of ENSO and the IOD and the mechanisms for impacts on Australian rainfall. J Clim 24:3910–3923. https://doi.org/10.1175/2011JCLI4129.1

Cai W, Zheng X-T, Weller E, Collins M, Cowan T, Lengaigne M, Yu W, Yamagata T (2013) Projected response of the Indian Ocean Dipole to greenhouse warming. Nat Geosci 6:999–1007. https://doi.org/10.1038/ngeo2009

Cai W et al (2018) Increased variability of eastern Pacific El Niño under greenhouse warming. Nature 564:201–206. https://doi.org/10.1038/s41586-018-0776-9

Eyring V et al (2016) Overview of the Coupled Model Intercomparison Project Phase 6 (CMIP6) experimental design and organization. Geosci Model Dev 9:1937–1958

Hafeez M, Frost AJ, Vaze J, Smith A, Elmahdi A (2015) A new integrated continental hydrological simulation system: an overview of the Australian Resource Assessment Modelling System (AWRAMS). Water v42:75–82

Hui C, Zheng X-T (2018) Uncertainty in Indian Ocean Dipole response to global warming: the role of internal variability. Clim Dyn 51:3597–3611. https://doi.org/10.1007/s00382-018-4098-2

Min SK, Cai W, Whetton P (2013) Influence of climate variability on seasonal extremes over Australia. J Geophys Res Atmos 118:643–654. https://doi.org/10.1002/jgrd.50164

Nicholls N, Lavery B, Frederiksen C, Drosdowsky W (1996) Recent apparent changes in relationships between the El Niño–Southern Oscillation and Australian rainfall and temperature. Geophys Res Lett 23:3357–3360. https://doi.org/10.1029/96GL03166

Rayner NA et al (2003) Global analyses of sea surface temperature, sea ice, and night marine air temperature since the late nineteenth century. J Geophys Res 108:4407. https://doi.org/10.1029/2002JD002670

Saji NH, Goswami BN, Vinayachandran PN, Yamagata T (1999) A dipole mode in the tropical Indian Ocean. Nature 401:360–363. https://doi.org/10.1038/43854

Shi G, Ribbe J, Cai W, Cowan T (2008) An interpretation of Australian rainfall projections. Geophys Res Lett 35:L02702. https://doi.org/10.1029/2007GL032436

Takahashi K, Montecinos A, Goubanova K, Dewitte B (2011) ENSO regimes: reinterpreting the canonical and Modoki El Niño. Geophys Res Lett 38:L10704. https://doi.org/10.1029/2011GL047364

Taylor KE, Stouffer RJ, Meehl GA (2012) An overview of CMIP5 and the experimental design. Bull Am Met Soc 93:485–498. https://doi.org/10.1175/BAMS-D-11-00094.1

Taschetto AS, England MH (2009) El Niño Modoki impacts on Australian rainfall. J Clim 22:3167–3174. https://doi.org/10.1175/2008JCLI2589.1

Ummenhofer CC et al (2009) What causes southeast Australia's worst droughts? Geophys Res Lett 36:L04706. https://doi.org/10.1029/2008GL036801

Van Dijk A. (2010) The Australian Water Resources Assessment System. Landscape Model (version 0.5). Technical Report 3. CSIRO. Australia.Van Dijk, A & Warren, G. 2010. The Australian Water Resources Assessment System. Technical Report 4. Landscape Model (version0.5) Evaluation Against. Observations. Technical Report. CSIRO. Australia.

Viney N, Vaze J, Crosbie R, Wang B, Dawes W, Frost A (2015) AWRA-L v5.0: technical description of model algorithms and inputs. CSIRO, Australia

Wang G, Cai W (2013) Climate-change impact on the 20th-century relationship between the Southern Annular Mode and global mean temperature. Sci Rep 3:2039

Wang G, Cai W, Santoso A (2020) Stronger increase in the frequency of extreme convective than extreme warm El Niño events under greenhouse warming. J Clim 33:675–690. https://doi.org/10.1175/JCLI-D-19-0376.1

Wang G, Hendon HH (2007) Sensitivity of Australian rainfall to inter-El Niño variations. J Clim 20:4211–4226. https://doi.org/10.1175/JCLI4228.1

Zelinka MD et al (2020) Causes of higher climate sensitivity in CMIP6 models. Geophys Res Lett 47:e2019L085782

Zheng XT et al (2013) Indian Ocean Dipole response to global warming in the CMIP5 multimodel ensemble. J Clim 26:6067–6080. https://doi.org/10.1175/JCLI-D-12-00638.1

Publisher's Note